ISSN 1590-8844
International Journal of Mechanics and Control, Vol. 17, No. 02, 2016

EXTERNAL AND INTERNAL CFD ANALYSIS OF A HIGH-SPEED HUMAN POWERED VEHICLE

Paolo Baldissera Cristiana Delprete

Politecnico di Torino, Department of Mechanical and Aerospace Engineering

ABSTRACT

Human powered vehicle competitions provide a stimulating research field aiming at the development of high-efficiency and sustainable means of transportation. Aerodynamic studies about top-speed bicycles, even if classified as sport engineering, are able to increase the knowledge also for the design of their commuting version such as three-wheeled velomobiles. In the present paper, some of the design and manufacturing features that play a key role in the aerodynamic performance of such vehicles are discussed. Then, a critical review of a case study prototype is presented and five CFD models of the same vehicle are compared and discussed. In particular, two aspects are investigated and quantified in terms of power loss: the negative effects of surface discontinuities on the laminar-turbulent transition of the boundary layer and the crucial role of wheel-wells for a properly working internal ventilation.

Keywords: CFD, HPV, Design, Sport, Cycling

1 INTRODUCTION

Although not included in classical sport disciplines and banned from traditional cycling, Human Powered Vehicles (HPVs) offer an interesting field for educational [1] and research purposes in many disciplines.

While the definition of HPVs indicates a wide general category of vehicles, it is well assessed by the last century results that full faired recumbent bicycles and tricycles are the fastest and the most efficient HPVs. The records sanctioned by national and international HPV associations [2,3] are often similar to traditional cycling such as the classic one hour travelled distance, the standing start kilometre and the flying start 200 m sprint for the top-speed. A special event in this field is the World Human Powered Speed Championship (WHPSC) [4] yearly held in Battle Mountain (Nevada, US). Here, the speed is averaged over a 200 m trap at the end of a quite flat segment (average slope −0.6%) of 8 km on the State Route 305. In September 2015 the Canadian rider Todd Reichert pushed the world record up to 139.45 km/h with the accurately designed and manufactured prototype Eta (Aerovelo Team) [5].

Contact author: Paolo Baldissera[1]

[1] Politecnico di Torino
Dept. of Mechanical and Aerospace Engeneering
Corso Duca degli Abruzzi, 24 - 10129 Torino, Italy
Email: paolo.baldissera@polito.it

Despite the measurement range corresponds to UCI (Union Cycliste Internationale) sprint, the effort is different. Each run requires 3-4 minutes of aerobic activity, around 1 minute of anaerobic power ramp and a maximal effort for the last 40-60 seconds: this is a longer and harder effort compared with the short-time needed in UCI 200 m sprint (current record 77.03 km/h, François Pervis, 2013 [6]).

Scientific papers about HPVs were published in the last decades focusing on many aspects such as ergonomics [7,8], aerodynamics [9-11] and high-speed handling [12]. Another valuable source of short technical information is the magazine collection Human Power [13].

The Policumbent Student Team [14] supervised by the authors had its debut at the WHPSC 2015. The rider Andrea Gallo set the Italian speed record of 116.19 km/h on the prototype PulsaR. The testing and racing experience has given the opportunity to understand both design and manufacturing limitations of the current project. As a consequence, a development program has been started in order to improve the current prototype and to develop a totally new design for challenging the world record in 2017.

In the present article the key aspects in aerodynamic design of high-speed HPVs will be discussed. Through Computational Fluid Dynamics (CFD) analysis with different focuses and modelling approaches on PulsaR, both external and internal flows will be analysed and discussed in comparison with the achieved speed.

2 KEY ASPECTS IN HPV AERODYNAMICS

In the design of full faired HPVs for top speed record attempts, a crucial role is played by the aerodynamic drag. In particular, two key aspects can determine success or failure in this field:

- the knowledge to design a shape with natural laminar flow and with the minimal volume fitting the rider size;
- the ability to keep the laminar flow in real world conditions.

These two aspects will be briefly discussed in the next paragraphs in order to point out vehicle design evolution and possible future developments.

2.1 LAMINAR FLOW DESIGN

The design of a streamlined body allowing for an extended laminar boundary layer at a given range of speed is a challenge that concerns many engineering applications dealing with different fluids.
The boundary layer around a body is defined as laminar when the air particles move in orderly way, which means in parallel layers with no mixing and eddies. When critical conditions are reached, the transition of the boundary layer from laminar to turbulent occurs and the flow starts to mix and to behave in irregular ways. The two conditions are represented in Figure 1 for an observer moving with the body wall. A laminar boundary layer results in a lower skin friction over the immersed body and provide a reduced drag with respect of the turbulent one. For this reason laminar design is a key factor in HPVs and in almost all sport competitions involving vehicle speed.

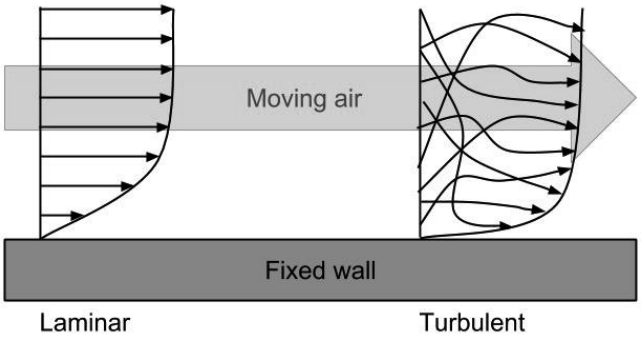

Figure 1 Laminar and turbulent boundary layers.

2.2 FROM THE VIRTUAL TO THE REAL WORLD

The second key point involves the ability to evaluate and to minimize the production imperfections and the external factors that could potentially undermine the original design. Some examples of manufacturing details that are potential sources of turbulence are:

- badly thermoformed front windscreen;
- non-smooth junction of the front windscreen or of any opening for the rider or for the maintenance;
- thick sponsor stickers on the fairing.

In practice, due to strict timeline and inexperience, all these considerations were neglected during the first manufacturing of PulsaR, as pointed out in Figure 2. In particular, the acrylic glass in the upper front of the vehicle was not properly thermoformed and assembled, likely resulting in a strong limitation of the laminar boundary layer extension.
Concerning external conditions in the real world, particular attention should be given to:

- lateral wind up to 6 km/h (legal limit from any direction for record validation);
- vibrations of the external fairing, coming from the road and through the vehicle frame.

Finally, the air flow entering and exiting from the vehicle can also affect its aerodynamic performance and is worthy of a specific discussion in the next paragraph.

2.2.1 Rider ventilation and internal flow

By enclosing the rider into an aerodynamic shell the need for a ventilation system arises. Such system has to meet the following requirements:

- to provide the right amount of oxygen for the required effort and weather conditions;
- to grant a proper temperature and humidity level;
- to ensure proper cooling for the brakes;
- to dry windows (if any) in order to avoid fogging;
- to minimize any additional drag.

The WHPSC competition rules then provide an additional requirement by excluding any additional source of energy for propulsion and for cooling (i.e. no ice-packs or heat storage systems). Ventilation through active fans is allowed only when the required energy is drained from muscular input and then subtracted from propulsion. In other words, the most natural solution is to have one or more air intakes and outlets working progressively with the vehicle speed.
Concerning the first requirement, the overall need in terms of air flow rate can be estimated by taking into account the kind of effort required and physiological data of the rider. The case of endurance disciplines requires to consider the large portion of ventilation aimed at cooling and drying the rider. Indeed, with an overall efficiency of about 25%, the human body deliver a heating power which is three times the mechanical power during cycling. It means that a professional cyclist giving 400 W of mechanical power for one hour will be dissipating 1200 W of power into heat. A detailed study about ventilation for cooling in endurance races can be found in [15].

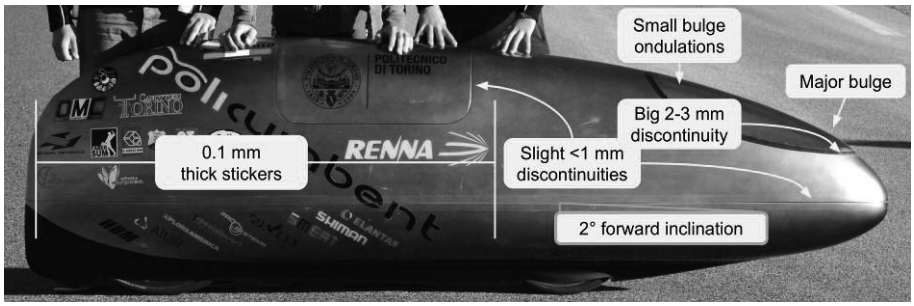

Figure 2 PulsaR 2015 with highlighted turbulent transition sources.

As a comparison, in [10] about 100 l/min are given as a general reference value for the air flow needed to breathe properly in maximal effort conditions, while the overall requirement can rise up to 1200 l/min for cooling the rider in case of endurance competitions.
Technical solutions for collecting and expelling the air in HPVs have some advantages and drawbacks. The practical experience of builders and riders attending the WHPSC suggests that:

- lateral NACA (National Advisory Committee for Aeronautics) ducts are an option, but can induce turbulent transition in the external flow and are more invasive than stagnation point intakes;
- wheel rotation significantly affects the overall drag, and it is strongly suggested to insulate them by means of dedicated wells;
- internal flow plays a not negligible role and is worthy of accurate study and implementation.

A common practice is to have a diffuser cone behind the intake hole in order to obtain a double effect: to reduce the air speed towards the rider and to recover the pressure drop on the nose of the vehicle. Indeed, frontal pressure on streamlined shapes is a double-edged sword: on the one hand it is a direct source of drag, on the other hand a certain amount of pressure is a requirement for the flow to stay laminar along a large portion of the vehicle body.

3 PULSAR CFD MODELS

The CFD analysis is a numerical technique for solving the Navier-Stokes equations that has been developed in the Aerospace and Automotive industrial fields. Thanks to the current accessibility of high computational resources at affordable prices, it is now applied to a wide range of fluid dynamics problems also in sports engineering such as nautical disciplines, from America's Cup [16] to kayak [17] and rowing boats [18-20], in swimming [21-23] and is a well-established method in cycling [24-31].
CFD analysis was used during the design phase of PulsaR in order to assess and optimize its shape. However, after the result obtained in September 2015 in Nevada with this prototype, the critical review and improvement of the CFD model was considered as a key activity for many reasons:

- to improve the model accuracy in assessing the PulsaR design limits in its ideal shape;
- to investigate the manufacturing errors and their possible solutions;
- to identify further potential improvements in order to push the vehicle at its potential top speed;
- to gain awareness of the intrinsic limitations of the vehicle shape in order to start a new project.

Since the above list of purposes involves the study of different phenomena and conditions, two groups of models were implemented in CD-Adapco StarCCM+®:

1. EXT group only considers the external flow over the closed volume of the fairing with the protrusion of the wheels;
2. INT group also includes the internal flow with a simplified representation of the inner structure, the rider and the rotating parts (Figure 3).

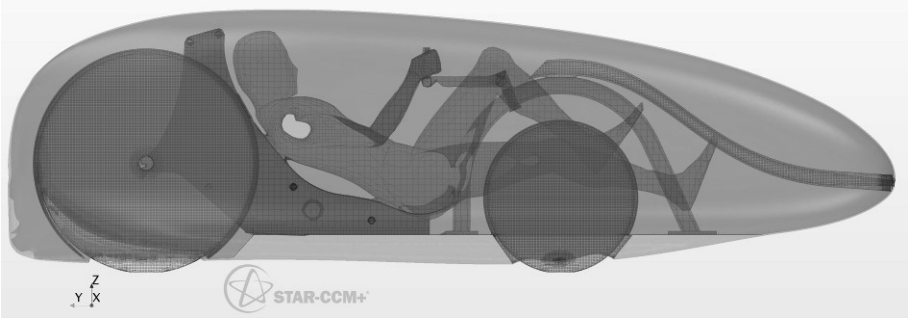

Figure 3 CFD mesh of the simplified internal elements for the INT-YW model (see Table I).

For both groups the simulations were performed at a speed of 125 km/h (as 2016 target) in open road conditions, which means in a large virtual tunnel of 25×6×8 m with PulsaR being 2.8×0.4×0.8 m (Figure 4). For all the models the ground was imposed as moving with the air and with no slip boundary condition.

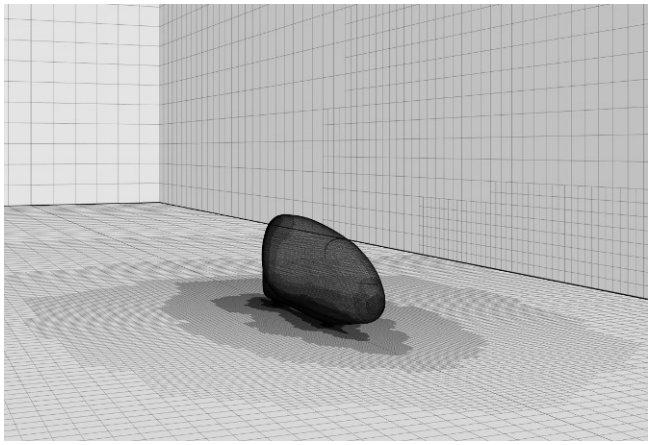

Figure 4 CFD mesh overview.

A speed-coherent rotation of the wheels (or of their protruding portion) was also imposed as boundary condition in both groups.
The EXT group includes three models:

1. EXT-A represents the perfect ideal shape of PulsaR in its horizontal alignment with respect to the ground and with a smooth continuous surface except for the protruding wheels. The model is aimed to an accurate evaluation of the laminar-turbulent transition, with a 30 prism layers for the boundary and Gamma-Re-Theta modelling for the transition;
2. EXT-B is an approximation of the manufactured shape of PulsaR 2015, with 2° forward inclination and bulgy windscreen having an irregular 2-3 mm misalignment with respect to the fairing surface (Figure 5). As for the previous, this model has 30 prism layers and Gamma-Re-Theta transition;
3. EXT-C has the same ideal geometry of model EXT-A, but is simulated with a Spalart-Almaras full turbulent model without laminar flow.

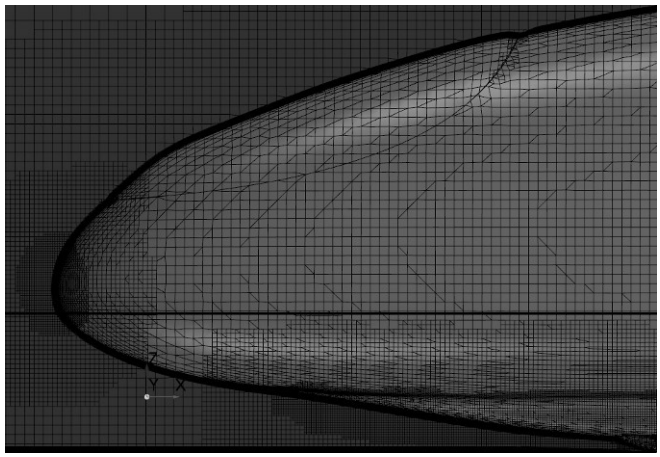

Figure 5 EXT-B model detail of the bulgy windscreen shape and steep junction.

The INT group, due to geometrical complexity and convergence stability, is not suitable for a transitional modelling. As a consequence its sub-models were calculated by using a fully turbulent boundary layer approach based on the Spalart-Almaras formulation. This group includes two models:

1. INT-NW has no wheel-wells as in the 2015 version of PulsaR;
2. INT-YW has front and rear wheel-wells with 7.5 mm clearance that insulates rather totally the rotational air flow from the inner volume, except for a small circular opening close to the rear hub.

A summary of the CFD models is reported in Table I.
For both EXT and INT groups a trimmer mesh was used plus the above mentioned prism layer, that was reduced to 3 levels in the case of the fully turbulent Spalart-Almaras simulations (EXT-C and the two INT models).
The meshing of INT models required the use of the wrapping function in order to identify and simplify the intersections among the various body inside the fairing.
The EXT group models resulted in mesh around 1.2 million cells by taking advantage of longitudinal plane symmetry, while the non-symmetrical INT group models required about 6.6 million cells to be carefully represented, even if the prism layer was limited to the fairing and to the tube.

Table I Summary of the CFD models and their characteristics.

Model	Description	Turbulence model	Transition model
EXT-A	External flow on perfect ideal surface	K-Omega	Gamma-Re-Theta
EXT-B	External flow, bulgy and misaligned windscreen, 2° forward inclination	K-Omega	Gamma-Re-Theta
EXT-C	External flow on perfect ideal surface	Spalart-Almaras	Fully turbulent
INT-NW	External and internal flow without wheel-wells	Spalart-Almaras	Fully turbulent
INT-YW	External and internal flow with both wheel-wells	Spalart-Almaras	Fully turbulent

4 CFD ANALYSIS RESULTS

All the simulations were run on 64 cores (AMD Opteron 2.3 GHz) over two nodes of a high performance computing cluster (ref. Acknowledgements). The EXT models converged in less than 1000 iterations with an overall CPU time of about 12 hours each, while the INT models converged after 1600 iterations for an overall CPU time of 56 hours each.
The results in terms of drag coefficient, force acting against the vehicle and equivalent power at 125 km/h of speed are summarized in Table II.

Table II Calculated drag coefficient, force and power at 125 km/h for the five implemented CFD models.

Model	Drag coefficient C_d	Total drag F_d [N]	Equivalent power [W]
EXT-A	0.0369	6.83	237
EXT-B	0.0505	9.34	324
EXT-C	0.0739	13.66	474
INT-NW	0.0826	15.30	531
INT-YW	0.0789	14.62	508

The results confirm the wide range of performance that can be achieved depending on the external flow conditions and provides useful indications about the role of the internal flow and the potential benefits from wheel-wells.
Moreover, a validation of the model comes from the coast-down measurements performed on a testing track with PulsaR in October 2015. Here, a drag coefficient C_d of 0.0834±0.010 was estimated from three repetition average and with an air density ρ of 1.1899 kg/m^3. Indeed, by considering the drag force F_d derived by definition of C_d and by applying the PulsaR frontal area of 0.259 m^2 it can be estimated for a speed of 125 km/h:

$$F_d = \frac{1}{2}\cdot\rho\cdot C_d\cdot A\cdot v^2 = 15.49\pm 0.37 \text{ N} \quad (1)$$

The obtained value is close to the CFD calculation with model INT-NW, which is in fact the most representative with respect to the tested prototype.
In the following, the specific information that can be argued by comparing the different models will be discussed separately for EXT and INT model groups.

4.1 EXTERNAL FLOW MODEL RESULTS

The drag estimations provided by EXT models A, B and C give support to the above mentioned key role of the manufacturing accuracy on the external surface. The drag resistance is doubled when passing from the maximum laminar boundary extension of model A to the fully turbulent boundary layer of model C. Model B represents a compromise between the other two, pointing out the remarkable influence of the windscreen imperfections on the transitional behaviour and on the final drag. As shown in Figure 6, the impact of such imperfections on the boundary layer is important and the laminar-turbulent transition is anticipated by the misaligned windscreen, especially in the top part of the fairing, where the potential laminar extension is maximum. The cost of this imperfection in terms of power is up to 87 W at 125 km/h.

The analysis points out that also the original design shape in its ideal condition has some limitations concerning the extension of laminar boundary layer. Indeed, the side of the vehicle is rather flat and does not allow to maintain a proper pressure gradient in order to avoid the transition.
Also, the last part of the tail shows an area with a drop in the wall shear stress (deep blue in upper Figure 6), suggesting a potential undesired detach of the flow.
All these considerations, together with the observation of the kind of shapes designed for the fastest prototypes such as the world record holder, provides valuable indications for developing the next speed-bike of the Team.

4.2 EXTERNAL-INTERNAL FLOW MODEL RESULTS

Before analysing the effect of the wheel-wells, it is interesting to discuss the increase in drag from model EXT-C to the INT models. While the EXT-C model represents a “worst condition” among the EXT group, it can be considered as “best ideal condition” with respect to INT models, at least within the fully turbulent approach. Model EXT-C represents the situation in which there is virtually no drawback from the inside flow on the external drag. From this perspective, model INT-NW estimates an increase of 1.64 N (+12%) of the overall drag, while the additional drag is reduced to 0.96 N (+7%) by mounting the wheel-wells as in model INT-YW. Assuming by hypothesis the same additional drag on the transitional model EXT-A the percentage increase is even bigger: +24% without wheel-wells and 14% with them.
In general, the additional drag at the simulated speed can be translated into additional power required for the rider by multiplying force and speed (125 km/h), leading to:

- +56.9 W without wheel-wells;
- +33.3 W with wheel-wells.

It follows that the use of wheel-wells can save 23.6 W at 125 km/h of speed, a significant amount of power when dealing with human effort and top-speed records. By plotting the power required to overcome the air drag as a function of the speed as in Figure 7, it is possible to visualize the improvement and eventually calculate the expected gain in top-speed by entering the measured or estimated 60 s sprint power of the rider on the vertical axis. As an example, the introduction of the wheel-wells could potentially provide an increase of 2 km/h, passing from 125 to 127 km/h with 530 W of power (to be summed to the power required to overcome the tyre rolling resistance). The improvement is clearly more important when passing to transitional models taking into account the portion of laminar boundary layer on the surface.

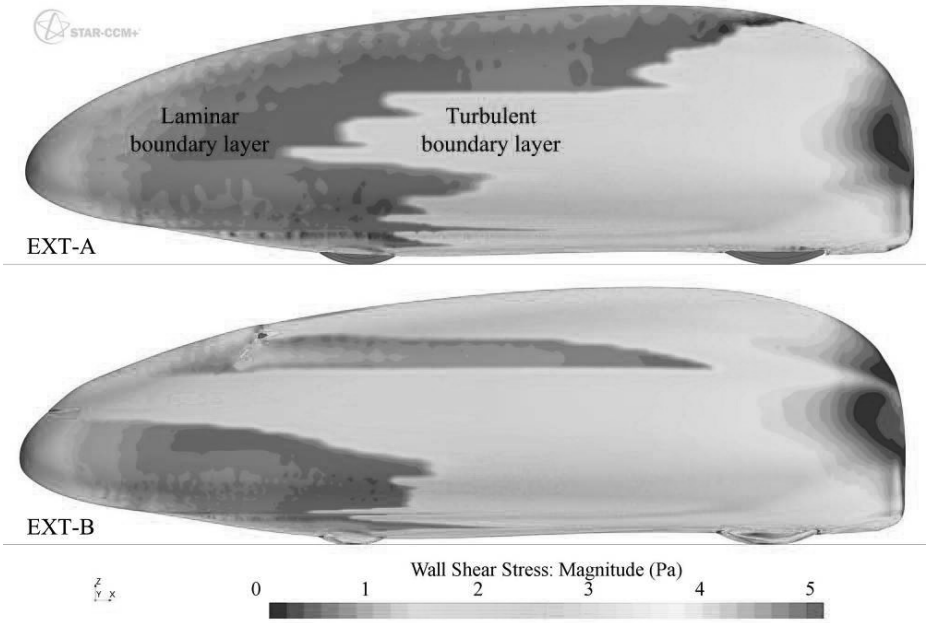

Figure 6 Wall shear stress and laminar boundary layer extension over EXT-A and EXT-B models.

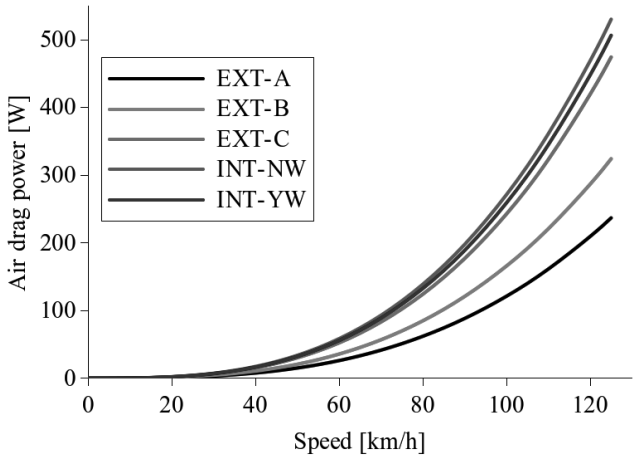

Figure 7 Power vs. speed curves of the CFD models.

Besides the gain in terms of drag, it is interesting to observe what the CFD analysis highlights about the behaviour of the flow inside the vehicle. As shown in Figure 8, the absence of wheel-wells produces a strongly randomized internal flow. Moreover, due to the proximity of the rear wheel to the air outlet cut, the behaviour of the latter is reversed. It means that the air is entering where it was originally designed to exit. This air is then summed to the air entering the front inlet and expelled through the wheels generating an increased turbulence in the bottom part of the vehicle, close to the ground, which is likely to increase the shear stress and thus the drag in that region. This result provides a useful information not only for the purpose of sport records, but also for the proper design of three-wheeled velomobiles [32] for daily commuting over an extended range with respect to standard bicycles. Such kind of vehicles, in many contexts, could represent the missing link between bicycle and cars as solution for a pollution free, healthy and safe personal mobility. One of their main limitation for the use in warm seasons and countries is exactly the internal ventilation to control the rider temperature and to extract the steam.

6 CONCLUSIONS

The key aspects for achieving high aerodynamic efficiency in HPVs were discussed with a focus on some manufacturing details. A critical review of an existing top-speed prototype (PulsaR 2015) was presented and five CFD models were implemented in order to quantify the role of the discussed features. In particular, a special focus was given to two topics, obtaining the following observations and estimations:

1. the surface smoothness and continuity is confirmed to play a crucial role in maintaining an extended laminar boundary layer over the vehicle and the presence of a small discontinuity in the windscreen junction can determine an increase of 37% in the coefficient of drag, which is potentially doubled in the worst case of a fully turbulent vehicle;
2. the use of internal wheel-wells can provide a significant improvement in the aerodynamic performance with a saving of 23.6 W of power at a speed of 125 km/h;
3. another important role of wheel-wells is to maintain a functional airflow inside the vehicle, avoiding the outlet cut to behave as an inlet and reducing the disturbance close to the ground.

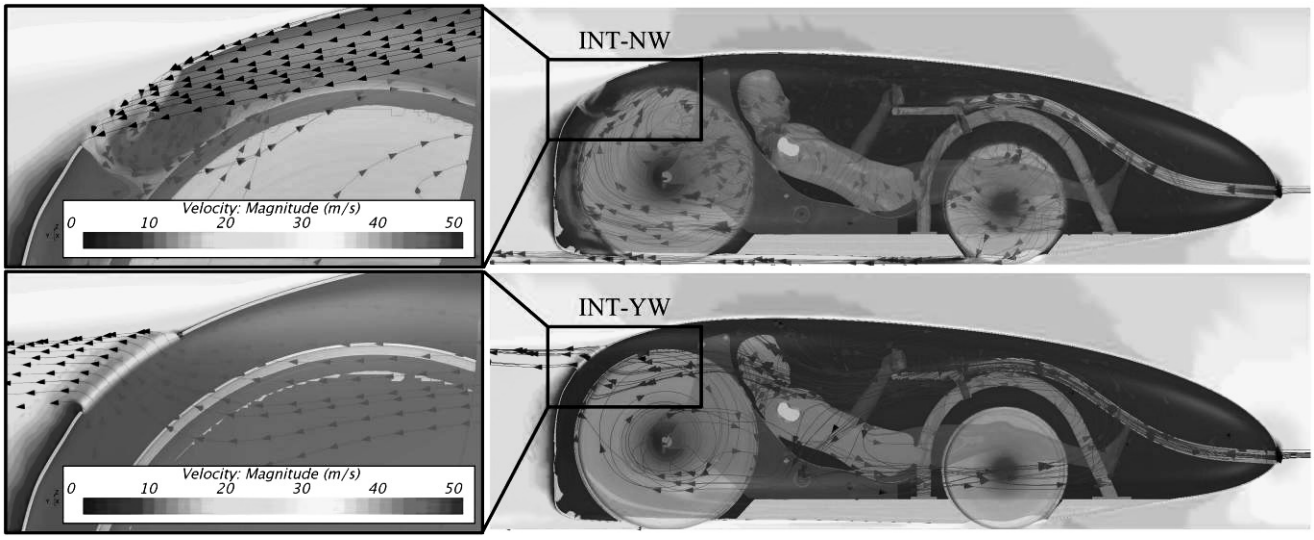

Figure 8 Overview and detail of the CFD calculated external and internal flow without wheel-wells (INT-NW) and with wheel-wells (INT-YW).

After horizontal realignment of the prototype through a fork spacer, replacement of the windscreen with a better one, accurate stuccoing of its junction and implementation of the only rear wheel-well, a rough 10% increase in top-speed was measured on PulsaR during a preliminary track test in Spring 2016. Further improvements and more detailed coast-down assessment are planned in June and July 2016, waiting for the WHPSC trials in Battle Mountain on September 12-17, 2016.

ACKNOWLEDGEMENTS

Computational resources were provided by HPC@POLITO which is a project of Academic Computing within the Department of Control and Computer Engineering at the Politecnico di Torino (http://www.hpc.polito.it).
StarCCM+ licenses were kindly provided by CD-Adapco as official partner of the Policumbent Team project.

REFERENCES

[1] Baldissera P., Delprete C., Human powered vehicle design: a challenge for engineering education. *Procedings of ESDA*, Copenhagen, June 25-27, 2014.

[2] www.ihpva.org, accessed on May 27, 2016.

[3] www.whpva.org, accessed on May 27, 2016.

[4] http://recumbents.com/wisil/whpsc2016/speedchallenge.htm, accessed on May 27, 2016.

[5] www.aerovelo.com, accessed on May 27, 2016.

[6] http://www.uci.ch/mm/Document/News/NewsGeneral/16/60/64/20151009_Historiquedesrecords_HommesElite_Neutral.pdf, accessed on May 27, 2016.

[7] Capelli C., Ardigò L., Schena F., Zamparo P., Energy cost and mechanical efficiency of riding a human-powered recumbent bicycle. *Ergonomics*, Vol. 51, No 10, pp. 1565-1575, 2008.

[8] Reiser II R., Peterson M., Broker J., Anaerobic Cycling Power Output With Variations in Recumbent Body Configuration. *Journal of Applied Biomechanics*, Vol. 17, No. 3, pp. 204-216, 2001.

[9] Kyle C., Burke E., Improving the racing bicycle. *Mechanical Engineering*, Vol. 106, No. 9, p.34, 1984.

[10] Kyle C. R., Weaver M. D., Aerodynamics of human-powered vehicles. *Proc IMechE Part A: Journal of Power and Energy*, Vol. 218, No. 3, 141-154, 2004.

[11] Epema H., Van den Brand S., Gregoor W., Kooijman J., Pereboom H., Wielemaker D., Van der Zweep C.-J., Bicycle Design: A different approach to improving on the world human powered speed records. *Procedia Engineering*, Vol 34, pp. 313-318, 2012.

[12] Patterson W., Leone G., The Application of Handling Qualities to Bicycle Design. *Proceedings of Bicycle and Motorcycle Dynamics*, pp. 1-10, 2010.

[13] *Human power - The technical journal of the international human powered vehicle association* (1977-2004). Accessed on May 27, 2016 at http://www.ihpva.org/hparchive.htm.

[14] www.policumbent.it, accessed on May 27, 2016.

[15] W.B. Schreur, *Human Power eJournal* (2004), published online on http://www.hupi.org, accessed on April 5, 2016.

[16] Nicolopoulos D., Berton E., Gouvernet G. et al., A hybrid numerical method to develop america's cup yacht appendages. *Sports Engineering*, 11(4), pp. 177-185, 2009.

[17] Banks J., Phillips A.B., Turnock S.R. et al., Kayak blade-hull interactions: A body force approach for self-propelled simulations. *Proc IMechE Part P: Journal of Sports Engineering and Technology*, Vol. 228, No. 1, pp. 49-60, 2014.

[18] Coppel A., Gardner T.N., Caplan N. et al., Simulating the fluid dynamic behaviour of oar blades in competition rowing. *Proc ImechE Part P: Journal of Sports Engineering and Technology*, Vol. 224, No. 1, pp. 25-35, 2010.

[19] Sliasas A. and Tullis S., Numerical modelling of rowing blade hydrodynamics. *Sports Engineering*, Vol. 12, No. 1, pp. 31-40, 2009.

[20] Sliasas A. and Tullis S., The dynamic flow behaviour of an oar blade in motion using a hydrodynamics-based shell-velocity-coupled model of a rowing stroke. *Proc IMechE Part P: Journal of Sports Engineering and Technology*, Vol. 224, No. 1, pp. 9-24, 2010.

[21] Bixler B. and Riewald S., Analysis of a swimmer's hand and arm in steady flow conditions using computational fluid dynamics. *Journal of Biomechanics*, Vol. 35, No. 5, pp. 713-717, 2002.

[22] Rouboa A., Silva A., Leal L. et al., The effect of swimmer's hand/forearm acceleration on propulsive forces generation using computational fluid dynamics. *Journal of Biomechanics*, Vol.39, No.7, pp. 1239-1248, 2006.

[23] Hayati A.N., Ghaffari H. and Shams M., Analysis of free-surface effects on swimming by the application of the computational fluid dynamics method. *Proc IMechE Part P: Journal of Sports Engineering and Technology*, published online before print, 2015.

[24] Blocken B., Defraeye T., Koninckx E. et al., CFD simulations of the aerodynamic drag of two drafting cyclists. *Computers & Fluids*, Vol. 71, pp. 435-445, 2013.

[25] Defraeye T., Blocken B., Koninckx E. et al., Aerodynamic study of different cyclist positions: CFD analysis and full-scale wind-tunnel tests. *Journal of Biomechanics*, Vol. 43, No. 7, pp. 1262-1268, 2010.

[26] Defraeye T., Blocken B., Koninckx E. et al., Computational fluid dynamics analysis of cyclist aerodynamics: Performance of different turbulence-modelling and boundary-layer modelling approaches. *Journal of Biomechanics*, Vol. 43, No. 12, pp. 2281-2287, 2010.

[27] Defraeye T., Blocken B., Koninckx E. et al., Computational fluid dynamics analysis of drag and convective heat transfer of individual body segments for different cyclist positions. *Journal of Biomechanics*, Vol. 44, No. 9, pp. 1695-1701, 2011.

[28] Defraeye T., Blocken B., Koninckx E. et al., Cyclist drag in team pursuit: Influence of cyclist sequence, stature, and arm spacing. *Journal of Biomechanics*, Vol. 136, No. 1, 2013.

[29] Griffith M.D., Crouch T., Thompson M.C. et al., Computational fluid dynamics study of the effect of leg position on cyclist aerodynamic drag. *Journal of Fluid Engineering - T ASME*, Vol. 136, No. 10, 2014.

[30] Fintelman D., Hemida H., Sterling M. et al., CFD simulations of the flow around a cyclist subjected to crosswinds. *Journal of Wind Engineering & Industrial Aerodynamics*, Vol. 144, pp. 31-41, 2015.

[31] Blocken B. and Toparlar Y., A following car influences cyclist drag: CFD simulations and wind tunnel measurements. *Journal of Wind Engineering & Industrial Aerodynamics*, Vol. 145, pp. 178-186, 2015.

[32] Baldissera P., Delprete C., Tirelli M., Velomobiles: design guidelines. *International Journal of Mechanics and Control*, Vol. 13, No. 2, pp. 41-49, 2012.